

# X-ray Thomson scattering studies on spin-singlet stabilization of highly compressed H-like Be ions heated to two million degrees Kelvin.

M.W.C. Dharma-wardana<sup>1,2,\*</sup> and Dennis D. Klug<sup>1,†</sup>

<sup>1</sup>*National Research Council of Canada, Ottawa, Ontario, Canada K1A 0R6*

<sup>2</sup>*Département de Physique, Université de Montréal, Montréal, Québec, Canada H3C 3J7*

Experiments at the US National Ignition Facility (NIF) [Döppner et al, *Nature* **618**, 270-275 (2023)] have created highly compressed hot hydrogen-like Be plasmas. Published analyses of the the NIF experiment have used finite- $T$  multi-atom density-functional theory (DFT) with Molecular dynamics (MD), and Path-Integral Monte Carlo (PIMC) simulations. These methods are very expensive to implement and often lack physical transparency. Here we (i) relate their results to simpler first-principles average-atom results, (ii) establish the feasibility of rapid data analysis, with good accuracy and gain in physical transparency, and (iii) show that the NIF experiment reveals high- $T$  spin-singlet pairing of hydrogen-like Be ions with near neighbors. Our analysis predicts such stabilization over a wide range of compressed densities for temperatures close to two million Kelvin. Calculations of structure factors  $S(k)$  for electrons or ions, the Raleigh weight and other quantities of interest to X-ray Thomson scattering are presented. We find that the NIF data at the scattering wavevector  $k_{sc}$  of  $7.89 \text{ \AA}^{-1}$  are more consistent with a density of  $20 \pm 2 \text{ g/cm}^3$ , mean ionization  $\bar{Z} = 3.25$ , at a temperature of  $\simeq 1,800,000 \text{ K}$  than the  $34 \text{ g/cm}^3$ ,  $\bar{Z} = 3.4$  proposed by the NIF team. The relevance of ion-electron coupled-modes in studying small  $k_{sc}$  data is indicated.

PACS numbers: 52.25.Jm, 52.70.La, 71.15.Mb, 52.27.Gr

## I. INTRODUCTION

Matter under extreme densities  $\bar{\rho}$ , temperatures  $T$  and pressures  $P$  occurs naturally in planetary interiors and astrophysical objects. They also occur as transient states that have to be probed on sub-nanosecond timescales [1–6] via cutting-edge experiments on high-energy-density materials relevant to experimental astrophysics [3], fusion physics [4, 5] and even for nuclear-stockpile stewardship requirements. The Fermi energies  $E_F$  of compressed matter are large, and although  $T$  (where we use energy units) may be nominally high,  $T/E_F$  is small and hence the name “warm-dense matter” (WDM) has been used for such highly-correlated energy-dense matter. X-ray Thomson scattering (XRTS) [7, 8] (using kilo-eV X-rays that penetrate dense matter) provides information on the microscopic quantum states and thermodynamic states of these WDM samples. For instance, while compressed hot silicon [2, 6, 9, 10] is of geophysical interest, highly compressed H, C [11, 12] and Be are of interest in inertial fusion experiments and in astrophysics. Meanwhile, WDM Aluminum has continued to be a benchmark material whose EOS and even the dynamic structure factor have been the topic of many studies [1, 13].

In this study we re-examine the recent XRTS experiment on highly compressed Be ( $7.5\text{--}35 \text{ g/cm}^3$ ) at temperatures close two million Kelvin ( $T \sim 150\text{--}160 \text{ eV}$ ) conducted at the US national ignition facility (NIF) [14]. Density functional theory (DFT) using  $N$  atoms, with  $N \sim 64 - 256$  coupled to molecular-dynamics (MD)

optimization of the ionic structure is one of the tools used in analyzing such XRTS data [15–17, 19] where, traditionally, an evaluation of the mean ionization  $\bar{Z}$  is needed [20]. This method, variously referred to as DFT-MD, KS-MD (Kohn-Sham MD) and QMD (quantum molecular-dynamics) [5] will be referred to here as QMD due to its brevity and wider usage. Finite- $T$  applications of QMD for  $T > E_F$ , where  $E_F$  is the Fermi energy, are prohibitively expensive for most laboratories as the basis sets needed for the DFT calculations increase rapidly with  $T$ . Other methods, e.g., path-integral Monte Carlo (PIMC) simulations [21, 22] are even more demanding for computer resources. Döppner et al [14] used QMD as well as average-atom (AA) methods and analyzed their XRTs data at  $k = 7.9 \text{ \AA}^{-1}$ . They concluded that the Be WDM created at the NIF had a density  $\bar{\rho} = 34 \pm 4 \text{ g/cm}^3$  at  $T = 160 \pm 20 \text{ eV}$ , with a mean ionization  $\bar{Z} = 3.4 \pm 0.1$ .

While a major objective of our study is to re-analyze the XRTS data of the NIF experiment and draw attention to the spin-singlet stabilization of the hydrogen-like state of Be atoms, an equally important objective is to demonstrate that such analyses can be done rapidly and economically using a full first-principles approach [23–25] while achieving an accuracy at least comparable to the best available published results using QMD, PIMC etc., on the NIF-Be study. This is important since the computationally expensive QMD and PIMC resources needed to analyze extreme states of matter used by the NIF team or by Dornheim et al are not available to most laboratories.

Average-atom models construct ions containing a set of  $n_b$  bound electrons, and carrying a mean charge  $\bar{Z}$ , while the nuclear charge  $Z_{nu} = \bar{Z} + n_b$ . Another objective, taken up in this paper is that  $\bar{Z}$  is a rigorous DFT concept. If AA models are based strictly on DFT, then a one-atom DFT model can be formulated. In such models,

\* Email address: chandre.dharma@yahoo.ca

† Email address: Dennis.Klug@nrc-cnrc.gc.ca

both electron- and ion- many-body problems are reduced using appropriate XC-functions for electrons and ions respectively, e.g., as in the neutral pseudo-atom (NPA) model [19, 23–25]. Relating the quantities calculated by such AA models to, say, PIMC calculations, and defining equivalent quantities for different approaches require care, and this too is addressed in this study where we use the NPA version of an average-atom. This is also referred to as a “one-atom” DFT approach, in contrast to the “N-atom” QMD approach.

All calculations presented in this paper take mere minutes, and used only a HP-Inspiron (2018) elitebook laptop, while a VASP [26, 27] simulation reported here was done elsewhere. Furthermore, the one-atom DFT approach for XRTS [17], and the use of the classical-map (CM) approach for a more rapid calculation of the structure factor of quantum electrons [28–30] adopted here provide a physical picture that may be lacking in purely numerical simulations. For instance, PIMC and QMD do not use the distinction between bound and free electrons, but the physical picture of the  $1s$ -bound electron and its delocalization, developed within the concept of mean ionization is very useful here.

A PIMC study of the NIF experiment by Dornheim et al [21, 22] also revises the NIF estimate and proposes  $\bar{\rho} = 22 \pm 2 \text{ g/cm}^3$  at a temperature of 155.5 eV. We conclude, in close agreement with the Dornheim et al, that the NIF-Be data are consistent with a density  $\bar{\rho} = 20 \pm 2 \text{ g/cm}^3$ ,  $T = 155 \pm 5 \text{ eV}$  and  $\bar{Z} = 3.25 \pm 0.01$ .

## II. THE NIF EXPERIMENT AND XRTS ANALYSES

A hohlraum compression of a Be capsule is achieved in the NIF experiment using 184 optical laser beams. A further eight laser beams generate  $\sim 8.9 \text{ KeV}$  X-rays from a zinc foil. They are used for the probe beam [14]. The scattered intensity at selected angles (i.e., for scattering vectors  $\vec{k}_{sc}$ ) is measured. The ratio of the elastic ( $el$ ) to the inelastic ( $inel$ ) contributions to the full scattering intensity, denoted by  $r(k) = I_{el}/I_{inel}$  at the wave vector  $\vec{k}$ , can be directly measured. Since the WDM is in a plasma state, we assume a uniform fluid and only the magnitude of  $\vec{k}$  is relevant for the data analysis.

We use atomic units with  $\hbar = m_e = |e| = 1$ , and  $T$  will usually be given in energy units of eV (1 eV=11,604K). We also define the electron- and ion- Wigner-Seitz radii  $r_s = [3/(4\pi\bar{n})]^{1/3}$ ,  $r_{ws} = [3/(4\pi\bar{\rho})]^{1/3}$ , where  $\bar{n}$  is the average free-electron density in the plasma, while  $\bar{\rho}$  is the average ion density. The number of free electrons per ion (experimentally measured using a Langmuir probe in low- $T$  plasmas) is  $\bar{Z}$ , with  $\bar{Z} = \bar{n}/\bar{\rho}$ . The Fermi wavevector  $k_F = (2\pi^2\bar{n})^{1/3}$  and the Fermi energy  $E_F = k_F^2/2$  are important scales of energy and momentum for the electron subsystem.

The temperature of the sample has been estimated [31] from detailed-balance considerations [8] applied to the

XRTS signal, although more extensive modeling is needed in two-temperature plasmas where the ion temperature  $T_i$  differs from the electron temperature  $T_e$  [17]. The use of the imaginary-time correlation function approach for two-temperature systems has been proposed in Ref. [18]. Several theoretical analyses of the NIF experiment [14, 21, 22, 32] are available, and some use the well-known Chihara decomposition [33] together with QMD calculations [16] or with the NPA [17, 19].

The PIMC [21] simulations do not need the Chihara decomposition. However, it should be noted that NPA calculations, as well as average-atom calculations, unambiguously yield a complete set of eigenfunctions with negative and positive energies  $\epsilon_\nu(r)$ , for liquid metals and plasmas (away from metal-nonmetal transitions). Hence the separation of the spectrum into a bound part and a free part is not an *ad hoc* procedure, nor is it dependent on any “chemical” models of valence theory, but depends on the AA model itself. This dependence can be pinned down to a unique result if the model is required to be fully consistent with DFT. There are systematic approaches available even near metal-nonmetal transitions and resonances, where partially delocalized electrons have to be accounted for [34]. Recent developments in PIMC calculations have enabled the study of such regimes (e.g., at metal-insulator transitions) *ab initio* [35]. Such simulations involve thousands of electrons, and are very expensive compared to one-atom DFT methods.

Dornheim et al introduce calculations of the Rayleigh weight  $R_w(k)$ , as well as the *el/inel* ratio  $r(k)$  as model-insensitive quantities for determining  $\bar{\rho}, T$  and other relevant information of the WDM state. Calculations of  $R_w(k), r(k)$  are easily available within the NPA approach used here. However, many of the quantities used in the PIMC analysis, e.g., the electron-ion structure factor  $S_{ei}(k)$ , do not correspond to the  $S_{ei}(k)$  used in the theory of electrons and ions that uses ions of mean charge  $\bar{Z}$  as one of the components, even if the  $\bar{Z}$  implicit in the PIMC calculation agrees with that of the AA calculation. In effect, PIMC uses a two-component fluid consisting of *nuclei* and electrons, and deals with the electron-nuclear structure factor  $S_{en}(k)$  involving all electrons, instead of  $S_{ei}(k)$  that includes only the free-electron cloud, as defined by Chihara [33]. These differences are further discussed below.

Since the scattered intensity is proportional to the *e-e* dynamic structure (DSF) factor  $S_{ee}(k, \omega)$ , all theoretical approaches reduce to a manipulation and simplification of  $S_{ee}$  together with  $S_{ei}$  and the ion-ion structure factor  $S_{ii}$ . Since ion-dynamics is not resolved in most experiments, the frequency-integrated structure factors  $S_{a,b}(k)$ ,  $a = e, i$  can be used where appropriate. We define below, frequently used quantities of interest. These include the elastic and inelastic components of  $S_{ee}(k)$  where the use of an appropriate value of  $\bar{Z}$  is implied in this separation,

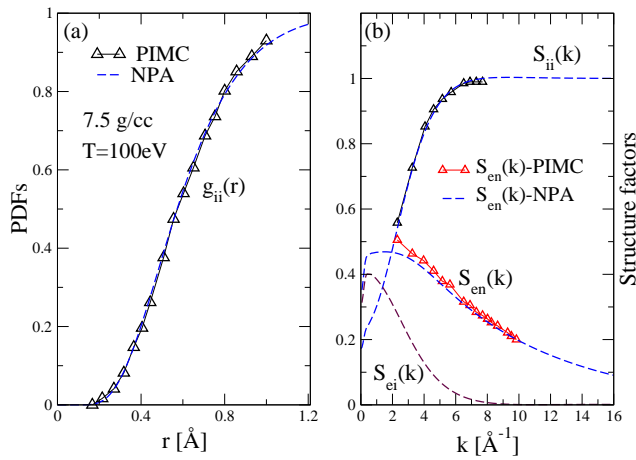


FIG. 1. (online color) (a) The NPA ion-ion  $g(r)$  (dashed line) for Be at 7.5 g/cm<sup>3</sup>,  $T=100$ eV compared with PIMC calculations (triangles) [21] (b) The ion-ion structure factor  $S_{ii}(k)$ , the electron-ion  $S_{ei}(k)$  and the electron-nuclear  $S_{en}(k)$  from NPA and PIMC.

as in Chihara’s approach [33].

$$S_{ee}(k) = S_{ei}(k) + S_{inel}(k) \quad (1)$$

$$r(k) = S_{ei}(k)/S_{inel}(k) \quad (2)$$

$$F_e(k) = \{n_b(k) + n_f(k)\} \quad (3)$$

$$F_I(k) = F_e(k)^2 S_{ii}(k) \quad (4)$$

Here  $F_e(k)$  is the electron form factor made up of the bound- and free- electron densities (in  $k$ -space), i.e.,  $n_b(k)$ ,  $n_f(k)$  respectively, obtained by Fourier transformation of  $n_b(r)$  and  $n_f(r) - \bar{n}$ . Furthermore,  $S_{ii}(k)$  is the ion-ion structure factor. This is the same as the nuclear-nuclear structure factor  $S_{nn}(k)$  obtained from expensive PIMC simulations of a mixture of, say, 25 Be nuclei and 100 electrons [21]. The last equation above, for  $F_I(k)$ , gives the so-called “ion-feature” used in XRTS studies.

In QMD, while the electron-electron many-body problem has been reduced to a one-body problem, the ion-ion problem has not been reduced in the same manner. Hence in QMD,  $N$ -atoms are placed in a simulation box and the multi-center Kohn-Sham electronic density  $n(\vec{r}, \vec{R}_1, \dots, \vec{R}_N)$  is calculated for each fixed ionic configuration  $\vec{R}_I$ ,  $I = 1$  to  $N$ , treated as a realization of a periodic crystalline solid. The ionic configurations  $\vec{R}_I$  are evolved using classical MD and a configuration average is taken to access physical quantities pertaining to the fluid state. In calculating the XRTS signal, or the mean ionization  $\bar{Z}$ , usually the  $N$ -atom output of QMD has to be decomposed into an average single-atom contribution, as discussed, e.g., in Plageman et al [16]. The  $\bar{Z}$  used in the NIF-study of Be is presumably based on the method of Bethkenhagen et al. [20].

We use QMD or PIMC only to establish benchmarks. For the bulk of the calculations we use NPA, a method that has been used in many studies since 1982, with details of practical implementations published in

Refs. [9, 24, 25], and validated by comparing with QMD, PIMC [11], and other calculations, even for dynamic structure-factor calculations [13]. We have shown in previous publications that the NPA which uses a single-nucleus-based DFT reduction of the many-ion and many-electron problem, yields the  $g_{ii}(r)$  and other quantities that agree very well with those obtained from QMD and PIMC. Furthermore, in the present study too we compare with the PIMC results of Dornheim et al, and give QMD results for Be using the Vienna Ab-initio Simulation Package [27], as detailed in the appendix.

In Figure 1 we compare our NPA calculations (whose details are given below) for Be at 7.5 g/cm<sup>3</sup> at 100 eV with PIMC calculations [21], showing good agreement. The  $S_{en}(k)$ -NPA, constructed from the NPA charge densities agrees with the PIMC  $S_{en}(k)$  in the relevant range of  $k$ , i.e.,  $k > k_F$ . The small- $k$  region is not accessible via PIMC due to limitations of simulation-box size. An approximate extension of  $S_{ei}(k)$  and  $S_{en}(k)$  for small- $k$  ( $< k_F$ ) presented in the figure uses an approximate two-component-fluid description discussed below, and in the appendix.

### III. NPA CALCULATIONS FOR THE NIF-BE EXPERIMENT

The details of the NPA calculation are well established [23–25]. However, we give a brief review of it in the appendix touching on how the number of free electrons per ion, viz.,  $\bar{Z}$  is determined via the Friedel sumrule and the minimization of the total free energy of the system.

#### A. Mean-ionization isotherms

In Fig. 2(a) we display the variation of  $\bar{Z}$  along isotherms  $T = 50, 100, 150$  and  $155$  eV. The significantly higher  $\bar{Z}$  estimate of Ref. [14] using QMD for  $T = 150$  eV is also shown (curve with asterisks).

The reasons for the overestimate of  $\bar{Z}$  in current QMD calculations have been noted and discussed in previous studies as well. DFT is a theory for the *total energy* and is not designed to give physical one-electron energies, occupations or bandgaps. These quantities (as calculated by most codes) contain self-interaction errors as well as discontinuities in the XC-functional that arise when an  $N + 1$  electron system becomes an  $N$ -electron system (see Kohn, Ref. [36]) interacting with an electron in a higher Kohn-Sham energy band, within a scheme of non-interacting Kohn-Sham electrons. These bands are non-physical DFT constructs; thus, normal-density Ge appears as a metal without a bandgap. As pointed out by Dharma-wardana [37], the calculations of  $\bar{Z}$  by Bethkenhagen et al [20] use DFT eigenstates and eigenvalues that are not corrected for these self-interaction effects and discontinuities in the XC-functionals. This is possibly the main reason for the difference in the values of  $\bar{Z}$  evaluated

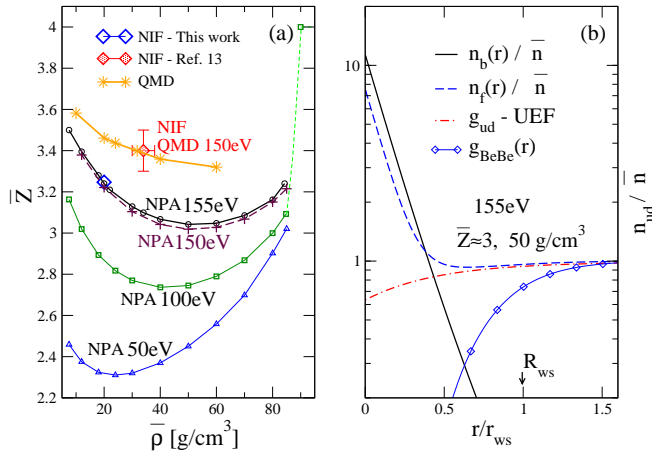


FIG. 2. (online color) (a) The NPA mean ionization  $\bar{Z}$  along four isotherms. The range of  $\bar{\rho}$  with  $\bar{Z} \approx 3$  widens as  $T$  increases. The  $\bar{Z}$  and  $\bar{\rho}$  estimates for the NIF-Be are indicated as ‘Diamond’ data points). The QMD estimates of  $\bar{Z}$ , Ref. [14] at 150 eV, (asterisks) are higher than NPA  $\bar{Z}$  at 150 eV estimates (+ symbol). The onset of full ionization to  $\bar{Z} = 4$  is shown for  $T = 100 \text{ eV}$  ( $\bar{\rho} \sim 85\text{--}90 \text{ g/cm}^3$ ). (b) The data for the case of a single electron (of specific spin) occupying the  $1s$  at  $155 \text{ eV}$ , viz.,  $50 \text{ g/cm}^3$  is displayed. The  $g_{\text{BeBe}}(r)$  penetrates the WS-sphere; thus the  $1s$  nearest-neighbour eigenstates will have opposite spin states (c.f., exclusion principle). The up-down e-e PDF for a uniform electron fluid (UEF) at the same  $\bar{n}, T$  (dot-dashed line) shows a weaker up-down enhancement at  $r = 0$ , but merges with  $n_f(r)/\bar{n}$  for  $r > r_{ws}/2$ .

via the NPA, and via QMD by Bethkenhagen et al, and via average-atom calculations [38]. Similarly, counting occupation numbers to obtain  $\bar{Z}$  from Kohn-Sham bound states is not formally justified, as the solution of a Dyson equation inclusive of GW-corrections [39] is needed.

Other authors, e.g., Gawne et al [40] have also discussed “quantifying ionization in hot dense plasma” using Kohn-Sham eigenstates. Alternative models based on transport properties have been examined, e.g., in Sharma et al [41] where a Born effective-charge model for the determination of  $\bar{Z}$  is proposed, without an *ab initio* construction of the underlying atomic model. More details of the evaluation of  $\bar{Z}$  in the NPA model using the Friedel sum rule at the minimum of the total Helmholtz free energy of the electron-ion system are given in the appendix. Some authors have (erroneously) claimed that  $\bar{Z}$  is not the mean value of any quantum operator and is hence not admissible in quantum calculations. We give its operator form in Sec. 2 of the Appendix, and also point out that the temperature  $T$  does not have a corresponding quantum operator in the usual sense.

Although the NPA  $\bar{Z}$  had reached close to 3.5 near  $7 \text{ g/cm}^3$ , compression does not push it to  $\bar{Z} = 4$ . Instead, the isotherms show a counter-intuitive *decrease* in ionization on compression, reaching towards more binding and then only proceeding to full ionization ( $\bar{Z} = 4$ ) at around  $\bar{\rho} > 80 - 85 \text{ g/cm}^3$ . Compression drives the field ions into the Wigner-Seitz cell of the central ion, as seen

from the  $g_{ii}(r)$  displayed in Fig. 2(b). At  $T = 155 \text{ eV}$ , Be-ions become closest to  $\bar{Z} = 3$  at about  $\bar{\rho} = 50 \text{ g/cm}^3$ . The only available bound state at  $155 \text{ eV}$  is the  $1s$  state, here calculated as the Kohn-Sham state  $\phi_{nl}(r), n = 1, l = 0$ . The corresponding  $n_b(r)$  is displayed in Fig. 2(b), for  $50 \text{ g/cm}^3$  at  $155 \text{ eV}$  and corresponds nominally to a single electron with a specific spin, say, up-spin in  $\phi_{1s}(r)$ . Its density, plotted on a log- $y$  scale is essentially linear. This density meets the field-ions within finite values of  $g(r)$ ; hence the nearest-neighbour  $\phi_{1s}$ , taken with an opposite spin would form a linear combination state that stabilizes the  $\bar{Z} = 3$  state. This also delocalizes the  $1s$  bound state from being a pure atomic state, into a state *partially bound to the ion distribution* as well. At lower temperatures, e.g.,  $100 \text{ eV}$ , the H-like Be with just one electron in the  $1s$ -state, with  $\bar{Z} = 3$ , occurs at  $80 \text{ g/cm}^3$ .

## B. XC-functionals

As the NPA is an all electron calculation which optimizes both the electron distribution  $n(r)$  and the ion distribution  $\rho(r)$  to minimize the Helmholtz free energy, it captures the best average-ion picture consistent with these electronic interactions brought in via the Hartree and the finite- $T$  XC-functional. The e-e XC functional of Perrot and Dharma-wardana (PDW) [30] is used in the NPA implementation. However, unlike PIMC simulations, the current implementation of the NPA does not use spin-density functional theory. The PDW e-e XC-functional used here [30] is based on the classical map for the electron fluid fitted to calculations in the range  $1 \leq r_s \leq 10$  with suitable analytic limits imposed for the Gellmann-Breuckner and Debye-Hückel limits. However, the fit to Quantum Monte Carlo data at finite- $T$  given by Karasiev et al [42], and by Groth et al, (GDS) [43] are expected to be more accurate, especially for  $r_s$  outside the fit range of the PDW version. Comparisons of  $F_{xc}^{ee}$  and  $V_{xc}$  using the the e-e XC functionals of GDS and PDW for the conditions of NIF-Be are given in the Appendix, and show some differences that do not produces significant differences in the final NPA calculations. Furthermore, in contrast, the QMD calculations seem to have simply used the  $T = 0$  XC-functional of Perdew, Burke and Ernzerhof [44]. These suggest that finite- $T$  XC-effects are of negligible importance for the NIF-Be conditions.

## IV. PAIR DISTRIBUTION FUNCTIONS AND STRUCTURE FACTORS

The compressed Be fluid with only  $1s$  occupation may be viewed as an electron fluid with strongly enhanced up-down e-e correlations. The e-e  $g_{ud}(r)$  for a uniform electron fluid (UEF) at the same  $T, \bar{n}$  as the Be-WDM at  $50 \text{ g/cm}^3, T = 155 \text{ eV}$ , calculated using the classical-map approach [28] is also shown in Fig. 2(b). The  $n_b(r)/\bar{n}$  approximates to  $g_{ud}(r)$  of the Be-WDM only for large-



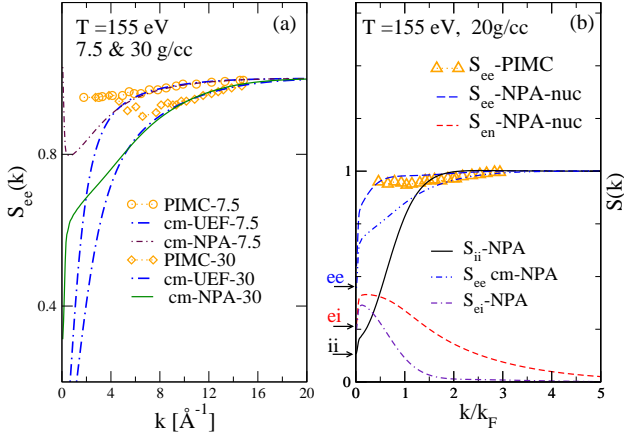


FIG. 3. (online color) (a) The  $S_{ee}(k)$  from PIMC, uniform-electron fluid (UEF), and from Eq. 5 for two densities, viz, 7.5 g/cm<sup>3</sup> and 30 g/cm<sup>3</sup>. The PIMC data are from ref. [21]. (b) The PIMC  $S_{ee}$  matched with  $S_{ee}$ -NPA-nuc constructed using Eq. 8. for Be at 20 g/cm<sup>3</sup> and  $T = 155$  eV.

$r > r_{ws}$ . It should be emphasized that the NPA calculation is independent of the classical-map calculation. The latter uses the value of  $\bar{Z}$  obtained from the NPA calculation to set the density parameter  $r_s$  used in the classical-map calculation.

The electron densities  $n(r) = n_b(r) + n_f(r)$  for  $T = 155$  eV,  $\bar{\rho} = 20$  g/cm<sup>3</sup> are relevant to our NIF-data analysis. They provides the densities used for NPA estimate of  $g_{ei}(r)$  and  $S_{ei}(k)$ . Since the NPA has provided the Kohn-Sham one-electron states  $\phi_\nu$ ,  $\nu = n, l$  for bound states, or  $k, l$  for continuum states, they can be used to construct an electron-electron response function from which the e-e structure factor  $S_{ee}(k)$  as modified by the ionic interactions could be obtained [45]. Thus all three static structure factors are in principle at our disposal from the NPA calculation. However, a more simplified calculation of  $S_{ee}$  inclusive of non-local XC-interactions can be obtained using the classical map (CM) of the electron-fluid [28, 30], using the  $\bar{Z}$  obtained from the NPA to construct the CM. More details are given in the appendix.

We note that the PIMC  $S_{ei}(k)$  does not extend to  $k < 2$  Å, presumably due to the limited size of the simulation box of the 25-atom sample. In Fig. 3 we display our NPA and classical-map based e-e structure factor  $S_{ee}^{cm}(k)$ , as well as NPA results for  $S_{ii}(k)$ ,  $S_{ei}(k)$ , for Be at 20 g/cm<sup>3</sup> and  $T = 155$  eV. The classical-map calculation [28] is for the interacting uniform electron fluid with a rigid uniform positive background; i.e., it is essentially a one-component calculation. This increasingly agrees with the two-component PIMC calculation as  $k$  increases, for  $k > k_F$ . The CM-calculation can be approximately extended to a two-component form (c.f. Chihara, Eq.38 of Ref. [33]) using the  $n_f(k)$ , and  $S_{ii}(k)$  from the NPA calculation. As such, the extended  $S_{ee}(k)$  are labeled as

cm-NPA- $\bar{\rho}$  for each density  $\bar{\rho}$  in the figure.

$$S_{ee}(k) = S_{ee}^{cm}(k) + S_{ii}(k)|n_f(k)|^2/\bar{Z} \quad (5)$$

$$S_{ei}(k) = n_f(k)S_{ii}(k)/\sqrt{\bar{Z}} \quad (6)$$

This Chihara extension obeys the compressibility sum-rule. That is, if  $\xi$  is the isothermal compressibility of the electron-ion fluid, then:

$$\bar{\rho}T\xi = S_{ii}(0) = S_{ei}(0)/\sqrt{\bar{Z}} = S_{ee}(0)/\bar{Z}. \quad (7)$$

Chihara's extension is an approximate model and not the result of a full two-component calculation. The latter is feasible with the classical-map hyper-netted chain (CHNC) procedure [28]. However, we have left this for a future study since the CHNC procedure itself has an ambiguity in assigning a temperature for the electron-ion interaction [29]. No such ambiguity exists in the NPA calculations.

It is seen that the Chihara extension of  $S_{ee}^{cm}(k)$  does not fully capture the  $S_{ee}(k)$  from PIMC. In panel (b) of Fig. 3 we display an extension of  $S_{ee}^{cm}(k)$  which is more successful in capturing the PIMC- $S_{ee}(k)$ . Here again we note that the PIMC is for a two-component mixture of electrons and nuclei. Hence we consider the forms:

$$S_{ee}(k) = S_{ee}^{cm} + S_{nn}(k)|n_f(k) + n_b(k)|^2/Z_{nu} \quad (8)$$

$$S_{en}(k) = S_{nn}(k)|n_f(k) + n_b(k)|/\sqrt{Z_{nu}} \quad (9)$$

$$S_{nn}(k) = S_{ii}(k) \quad (10)$$

Here  $S_{nn}(k)$  is the nuclear-nuclear structure factor, and  $Z_{nu}$  is the nuclear charge. The  $S_{nn}(k)$  of the PIMC calculation is identical with the  $S_{ii}(k)$  of NPA calculation provided that the  $\bar{Z}$  estimate implicit in the PIMC calculation agrees with that of the NPA. The  $S_{ee}(k)$  from PIMC and cm-UEF for two densities, viz, 7.5 and 30 g/cm<sup>3</sup> are displayed. Note the different small- $k$  behavior of the PIMC  $S_{ee}(k)$  and the CM- $S_{ee}$ . The 30 g/cm<sup>3</sup> curve follows the classical-map result up to about 5 Å<sup>-1</sup>, i.e,  $k \sim k_F$ , and deviates upwards and gives a small- $k$  behavior similar to that of the 7.5 g/cm<sup>3</sup> case. Setting  $S_{nn} = S_{ii}(k)$ , we can evaluate  $S_{ee}(k)$  using Eq. 8 to get the curve labeled “ $S_{ee}$ -NPA-nuc” to compare with the PIMC- $S_{ee}(k)$ . This Eq. 8 closely approximates the PIMC- $S_{ee}$  and reveals its physical content and its difference from Eq. 5

The CM- $S_{ee}(k)$  does not include the response of the ion-distribution as the UEF assumes a rigid neutralizing background. However, if the ion distribution is included as in a two-component plasma, the major effect is on the small- $k$  region where ion-acoustic coupled modes are formed and it affects all the response functions  $S_{ab}(k)$ ,  $a, b = e, i$  to the appropriate degree. The ion-acoustic coupled modes are of such long wavelength that PIMC simulations with 25 Be atoms cannot capture them. Their effect is to modify the small- $k$  behavior of  $S_{ee}(k)$  and in fact enforces the compressibility sum rule. However, these effects do not significantly affect our Rayleigh weight calculation, since the XRTS scattering  $k = 7.89$  Å<sup>-1</sup> in the present case is in the high- $k$  regime.

## V. CALCULATION OF THE RAYLEIGH WEIGHT

Dornheim et al [22] propose to use their calculated  $S_{ei}(k)$  and  $S_{ii}(k)$  to calculate the Rayleigh weight  $R_w$  defined by them as

$$R_w(k) = S_{ei}(k)^2 / S_{ii}(k). \quad (11)$$

As the PIMC calculations are for a two-component system of electrons and nuclei, as discussed in the context of Fig. 3, we note that their  $S_{ei}(k)$  is  $S_{en}(k)$  and it includes both bound electrons and free-electrons; hence it is more appropriately denoted as  $S_{en}(k)$ . Furthermore, it is *not* the same as  $S_{ei}(k)$  derived from  $g_{ei}(r) = n_f(r)/\bar{n}$  normally discussed within NPA/AA models as well as in Chihara's theory. The structure factors obtained from the bound- and free- electron densities  $n_b(k), n_f(k)$  associated with a single nuclear center as calculated by the NPA as well as via AA procedures need to be extended to reflect the two-fluid structure of the system [46], as briefly discussed in the appendix. However, for  $k > k_F$ , the following definition of the Rayleigh weight seems to be adequate and consistent with the form used by Dornheim et al, viz., Eq. 11 when using quantities calculated via the NPA or AA models.

$$R_w(k) = \{n_b(k) + n_f(k)\}^2 / \{\bar{Z} S_{ii}(k)\}. \quad (12)$$

In fig. 4 we compare our  $R_w(k)$ , Eq. 12 based on an ion-electron fluid, with the calculations of Dornheim et al [21] based on PIMC and QMD simulations for a nuclei-electron fluid, Eq. 11. The figure shows that the results of the NPA calculations, obtained via methods very different to the PIMC and QMD calculations provide strong support to one another as they agree and fall well within the likely error estimates of the two methods.

The scattering wavevector at  $k_{sc}=7.89 \text{ \AA}^{-1}$  corre-

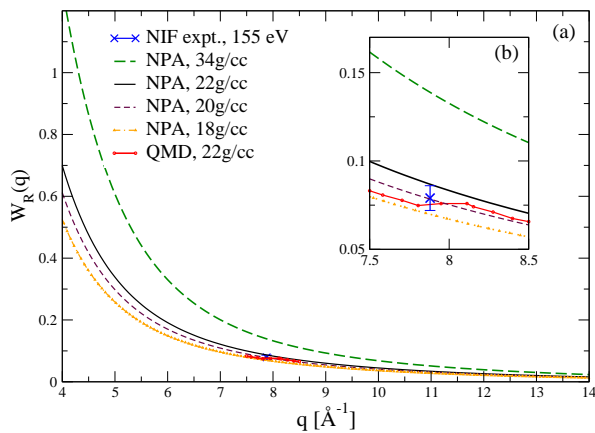


FIG. 4. (online color) (a) Rayleigh weight calculations for the NIF-XRTS signal at  $k_{sc}=7.89 \text{ \AA}^{-1}$  compared with QMD calculations of Dornheim et al, see Fig.3 of Ref. [22]. The inset (b) gives an expanded view near our NIF-Be estimate.

eV, and  $\bar{Z} = 3.247$ . It should be noted that while results for smaller scattering vectors, e.g., for  $k_{sc} < k_F$  would reveal more information on correlated behavior, these fall increasingly into the regime where ion-density fluctuations and electron-density fluctuations form coupled modes (ion-acoustic modes). Typical plots (Fig. 3, 4 of Ref. [47]) of the frequency-dependent e-e and i-i structure factors (Figs. 3, 4) and the relevant theory for quantum systems are given in Ref. [47]. The theory for weakly-coupled classical two-component electron-ion systems inclusive of coupled-mode formation, and including quantum-diffraction effects is given in Gregori et al [7].

The study of the small- $k$  scattering regime will increasingly require two-component plasma models constructed using the outputs of the usual NPA or AA calculations. Similarly, PIMC calculations and QMD will need very-large simulations consistent with the long-wavelength nature of ion-acoustic modes if small- $k$  scattering data are to be treated.

## VI. TRANSPORT PROPERTIES

The transport properties of Be at the high compressions and temperatures that appear in the NIF-study are of interest, and involve electron scattering from the ions, rather than photon scattering. While the coupling of the electrons to photons is weak and can be treated semi-classically, the scattering of electrons from the electron-ion system involves strong scattering effects, especially since the internal structure of the hot Be-ions no longer supports Pauli blocking. Hence the electrical conductivity  $\sigma$  and the thermal conductivity  $\kappa$  have to be evaluated via a T-matrix calculation. As  $\bar{Z}$  is large, electron-electron scattering effects may be neglected [48]. Our calculations for  $\sigma$  and  $\kappa$  for Be, following the method of Ref. [49] are presented in Fig. 5 for the three isotherms 50, 100 and 155 eV.

## VII. DISCUSSION

We have shown that the neutral-pseudo-atom model, i.e., a rigorous DFT-based average-atom model provides rapid and accurate interpretation of XRTS measurements, giving results in close agreement with more numerically demanding and costly methods like PIMC or  $N$ -atom QMD simulations. QMD calculations in the density and temperature range of the NIF experiment would consume months of computational time, while the NPA and other AA-methods take only minutes. Here we have shown that the NPA achieves results comparable to the PIMC and QMD calculations. Most AA codes could achieve similar or better accuracy by adhering more closely to density-functional theory.

The introduction of the Rayleigh weight  $R_w(k)$ , and the elastic to inelastic ratio  $r(k)$  etc., in recent publications [22] makes the exploitation of XRTS data via

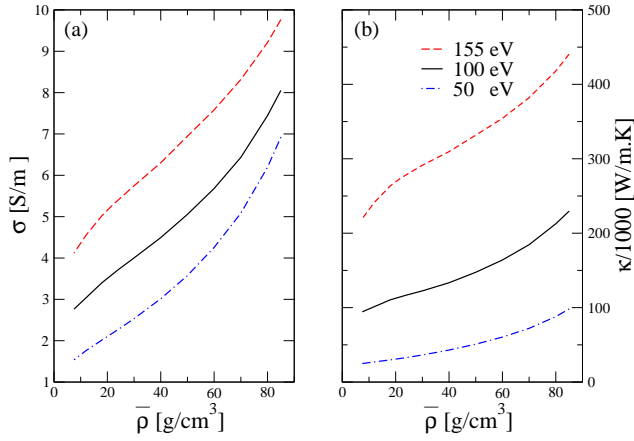


FIG. 5. (online color) (a) The electrical conductivity of Be at 50, 100 and 155 eV, for the range of densities  $\bar{\rho}$  in the range 5-85 g/cm<sup>3</sup>. (b) The thermal conductivity for Be plasmas of panel (a) calculated using the finite- $T$  Lorenz-number formalism of Ref. [49]

NPA/AA techniques even simpler. Furthermore, unlike PIMC or QMD, the scattering wavevector  $k$  of the XRTS signal accessible via NPA is not limited by the “box-size” of the simulations.

While NPA can (at least in principle) provide all the structure factors  $S_{a,b}(k)$ , with  $a, b$  = electrons or ions, the use of a classical map for calculating the  $S_{ee}(k)$  reduces computations to mere minutes, eminently implementable in “on-the-fly” calculations within large codes. Unlike QMD or PIMC, the NPA approach directly yields precisely definable single-ion properties such as the mean ionization  $\bar{Z}$ , the chemical potentials of ions and electrons, the minimum value of the free energy of the system and all related physical properties. By confirming the agreement of the NPA predictions of the Rayleigh weight etc., (here, via XRTS measurements), we validate  $\bar{Z}$  and other one-body properties of the average-atom model used in the NPA. This is merely a corollary of the DFT prescription that a complete one-body description in terms of  $n(r)$ ,  $\rho(r)$  and their exchange-correlation functionals exists by virtue of Mermin’s extension of the Hohenberg-Kohn theorem.

Unlike PIMC which is limited to low- $Z$  materials and higher temperatures, the NPA and classical-map methods are seamlessly applicable from very low to high temperatures. An exhaustive discussion of the equation of state of Be using the NPA was given by Perrot in 1993 [24], for compressions up to six, and  $T$  up to 100 eV. Perrot had also confirmed the 0-Kelvin isotherm and examined the application of the NPA to solid Be. More details of moderate- $T$  states of Be, ionization data up to 155 eV and 85 g/cm<sup>3</sup>, and comparisons with QMD calculations are given in the appendix.

## Appendix A

In this appendix we use the notations, abbreviations and units used in the main text.

### 1. Details of the NPA calculation

We consider a sphere of radius  $R_c = 10r_{ws}$  at low temperatures (i.e.,  $T/E_F \leq 1$ ). This is called the correlation sphere and it is sufficiently large such that all PDFs  $g_{ab}(r)$  have reached unity as  $r \rightarrow R_c$ . This is a significant difference from many popular AA models which use an ion-sphere of radius  $R_c = r_{ws}$  as the volume of the pseudoatom. The thermal de Broglie length  $\lambda_{deB}$  of electrons at temperature  $T$  in energy units is given by  $\lambda_{deB} = 1/(2\pi\bar{m}_e T)$ , where  $\bar{m}_e$  is the effective mass of the electron. As  $T \rightarrow 0$ ,  $\lambda_{deB}$  diverges to large values exceeding  $r_{ws}$ . Hence, electrons cannot be meaningfully confined to within an  $r \leq r_{ws}$  except at sufficiently high  $T/E_F$ . Thus the use of the ion-sphere model for average atoms is justified only for sufficiently large  $T/E_F$ .

The chemical potential  $\mu$  used in ion-sphere AA models is determined by an equation of the form

$$Z_n = \int_0^{r_{ws}} 4\pi r^2 n(r) dr \quad (A1)$$

$$n(r) = \sum_{\nu} 2(2l+1) |\phi_{\nu}(r)|^2 f(\epsilon_{\nu}, T) \quad (A2)$$

$$f(\epsilon_{\nu}, T) = 1/[1 + \exp\{(\epsilon_{\nu} - \mu)/T\}]. \quad (A3)$$

Here  $\phi_{\nu}$ ,  $\epsilon_{\nu}$ , with  $\nu = n, l$  or  $k, l$  are the bound and free eigenfunctions and eigenvalues of the spin-unresolved AA calculation, and  $n(r)$  is the total electron-density pileup inside the ion sphere. The so-evaluated  $\mu$  contains an increasingly large unphysical non-local potential that confines the free electrons within the ion sphere as  $T \rightarrow 0$ . This also implies that the  $\bar{Z}$  calculated from the Friedel sum rule for these ion-sphere AA models may even exceed the nuclear charge [38], where as it should equal  $\bar{Z} \leq Z_n$ .

Furthermore, a proper DFT model should have  $\mu$  equal to the non-interacting value  $\mu^0$ . So, the inclusion of this type of nonlocal potential in the calculation via a boundary condition (c.f., Eq. A1) implies that the Euler-Lagrange condition for the minimum of the total free energy of the electron-ion system implied by the Kohn-Sham equation is not met. A variety of ways has been proposed [50, 51] for the evaluation of  $\bar{Z}$  from such AA models. This ambiguity should be viewed as a weakness in such models rather than in the concept of ‘mean ionization’ as such.

The NPA does not use the ion-sphere, but works with a correlation sphere with a radius  $R_c$  typically 5 to 10 times  $r_{ws}$ , large enough to include all the particle correlations that exist in the physical system. Thus the correlation sphere nominally contains about 4000 Be nuclei and 16,000 electrons. For low-density high- $T$  plasmas, the correlation sphere becomes similar to the De-

bye sphere. For high  $T$  implementations, the correlation-sphere radius  $R_c$  may in practice be reduced to about  $5r_{ws}$ . One of the nuclei is at the origin of the coordinates; the field-nuclei (together with any bound electrons) are replaced by their (initially unknown) smoothed average ion-density distribution  $\rho(r) = \bar{\rho}g_{ii}(r)$ , each ion carrying a charge  $\bar{Z}$  which is to be determined self-consistently to reach a minimum in the Helmholtz free energy. Similarly, the electron density is  $n(r) = \bar{n}g_{ei}(r)$  and normally involves the “free” electron distribution  $n_f(r)$  that tends to  $\bar{n}$  as  $r \rightarrow \infty$ ; i.e., as  $r \rightarrow R_c$  and not  $r_{ws}$ . The bound electron distribution  $n_b(r)$  is short-ranged. A simple cavity-like trial  $g(r)$  for ions is specified by its radius  $r_{ws}$ , itself to be determined self-consistently with  $\bar{Z}$ ,  $n(r)$  and  $\rho(r)$  [23, 25]. As the NPA is a DFT model, the electrons are mapped to a non-interacting system at the interacting density. Hence, the chemical potential of the electrons is just the non-interacting value  $\mu^0$ .

The DFT calculation is based on a minimization of the Helmholtz free energy  $F([n], [\rho])$  via the coupled Euler-Lagrange equations for the electron distribution and the ion distribution.

$$\frac{\delta F([n], [\rho])}{\delta n} = 0, \quad (\text{A4})$$

$$\frac{\delta F([n], [\rho])}{\delta \rho} = 0. \quad (\text{A5})$$

The first of the above equations reduces to the Kohn-Sham equation for electrons in the correlation sphere. The second reduces to a DFT equation for classical particles. This can be reduced to a form of the modified hypernetted chain equation or treated via molecular dynamics. These equations (A4,A5) are discussed in some detail in Ref.[23, 24] and in Refs. [25, 52]. The main approximation made is the neglect of XC-potentials arising from certain electron-ion XC-functionals of the form  $F_{xc}^{ei}([n], [\rho])$  in most NPA calculations which retain  $F_{xc}^{ee}$  and  $F_{xc}^{ii}$ . The latter is highly non-local but an explicit form can be given in terms of  $g_{ii}(r)$ , Eq. 3.4 of Ref. [23].

How to include  $F_{xc}^{ei}$  in NPA calculations (if needed) is discussed in Ref. [46]. In fact, the main criticism against the NPA leveled by Chihara [53] is based on the neglect of  $F_{xc}^{ei}([n], [\rho])$  type XC-corrections. However, comparisons of PDFs, structure factors and other properties of WDM systems calculated from the NPA, with those from more microscopic methods show that the approximations used in the NPA are satisfactory.

Furthermore, for systems near metal-insulator type transitions, the issue of partially localized electrons (“hopping electrons”) needs to be treated, as in Ref [34]. However, the present study on Be is in the dense metallic region and hence “hopping electrons” are not an issue here. Instead, we have an unusual example of the “metal-lization” of even the 1s shell by delocalization into neighboring atoms.

The converged DFT equations A4,A5 for electrons and ions respectively define a minimum in the total free energy, inclusive of all many-body corrections that

are accounted for via the appropriate e-e and i-i XC-functionals. Thus a sophisticated Saha equation is automatically solved in evaluating the electron distribution  $n(r) = n_b(r) + n_f(r)$ , the ion distribution  $\rho(r)$  and the mean ionization  $\bar{Z}$ . At the end of the calculation we have  $g_{ii}(r)$ ,  $g_{ei}(r)$ , corresponding  $S_{ii}(k)$  and  $S_{ei}(k)$  where the  $k \rightarrow 0$  limit is accurately accessible, unlike in QMD and PIMC where the small size  $L \sim N^{1/3}$  of the simulation cells limit the  $k$  range to  $k > \pi/L$ .

The total free-energy is used to obtain the pressure, internal energy, compressibility and other EOS data. These, calculated from the NPA for Be are given in Ref. [24], for lower compressions ( $< 6$ ) and  $T \leq 100$  eV.

## 2. Evaluation of the mean ionization $\bar{Z}$ in the NPA

It has sometimes been claimed that the mean ionization  $\bar{Z}$  is not a properly defined quantity as “it cannot be given as *the mean value of a quantum operator*” [41, 54–56], or that it is a “a heuristic” quantity [21]. The ‘temperature’  $T$  also has no operator in quantum mechanics; hence, although the same claim could be used against  $T$ , those who reject  $\bar{Z}$  continue to retain  $T$  in their theories. We are in fact *not* studying pure quantum systems, but our interest is in quantum-*statistical* systems where a classical heat bath is attached to the quantum system. The temperature  $T$ , chemical potential  $\mu$ , and  $\bar{Z}$  appear as Lagrange multipliers in the quantum-statistical theory used [23]. Furthermore, one may invoke extended field-theoretic formulations of quantum statistical theory, e.g, thermofield dynamics [57], where operator formulations are available for quantities like  $T$ ,  $\mu$  and  $\bar{Z}$ . However, for the case of  $\bar{Z}$ , it is possible to give an operator form even within standard quantum theory using the phase shifts of plane waves scattering off a pseudoatom. The Friedel sumrule, to be discussed below is in fact an embodiment of that approach.

On convergence, NPA calculation satisfies the finite- $T$  Friedel sum rule [23] accurately and provides the value of  $\bar{Z}$  adopted in our calculations. The NPA provides the phase shifts  $\delta_l(k)$  of the continuum eigenstates, with energy  $\epsilon(k, l) = k^2/2$  which is independent of  $l$ . The  $l$  states are evaluated up to an  $l_{max} \sim 30$  or as appropriate.

$$\bar{Z} = \frac{2}{\pi T} \int_0^\infty dk k f(k) \{1 - f(k)\} \hat{X} \quad (\text{A6})$$

$$\hat{X} = \sum_l (2l+1) \hat{\delta}_l(k) \quad (\text{A7})$$

$$f(k) = 1/\{1 + \exp(k^2/2 - \mu^0)/T\} \quad (\text{A8})$$

Noting that  $f(k)(1 - f(k))$  can be expressed as the derivative of the Fermi function, Eq. A6 can be written as the meanvalue  $\langle \hat{X} \rangle$  where both a thermal and a quantum mechanical average are taken over the scattering operator  $\hat{X}$ , defined in terms of the phase shifts  $\hat{\delta}_l$ . Here the phase shift  $\hat{\delta}_l$  is not just a number but the operator that modifies the scattering amplitude. The phase shifts are



viewed as operators acting on the incoming wavefunctions, modifying their phases and creating the outgoing wavefunction in each channel.

So, contrary to claims that  $\bar{Z}$  is a quantity without an operator representation, inadmissible in quantum theories, we regard it as a Lagrange multiplier for charge neutrality [23], having an operator representation and a quantum-statistical meanvalue that arises in the DFT projection of the  $N$ -atom density to a single average atom. Just as the one-body eigenvalues, eigenfunctions etc., of DFT theory refer to properties of the non-interacting Kohn-Sham electron system, the  $\bar{Z}$  and other properties of the NPA belong to the non-interacting system of pseudoatoms of DFT theory. This approach consistently provides the total Helmholtz free energy of the system, and related finite- $T$  thermodynamic and linear transport properties of WDM systems [49].

XRTS may be considered as an experimental means of measuring  $\bar{Z}$  of matter under extreme conditions, while Langmuir probes can be used for measuring the free electron density per ion (i.e.,  $\bar{Z}$ ) in low- $T$  plasmas. Fit formulae for  $\bar{Z}$  for Be as a function of density for six isotherms in the range (1 eV to 155 eV) are given in sec. A 4.

### 3. The atomic structure of Be at 20g/cm<sup>3</sup> and 155 eV

As seen in Fig. 4, our calculations suggest that the NIF-Be sample had a density of 20 g/cm<sup>3</sup> and a temperature of 155 eV. A plot of the NPA bound and free-electron densities obtained is displayed in Fig. 6.

The all-electron Kohn-Sham calculation gives only a  $1s$  bound state with an energy  $\epsilon_{1s} = 4.5605$ , and a mean radius  $\langle r \rangle = 0.4182$  a.u., while the nominal Wigner-Seitz radius is 1.064 a.u. Hence, the  $1s$ -state is mostly contained in the WS-sphere. Nevertheless, as seen in Fig. 1(b), at these compressions, the ion-ion pair-distribution function has a significant presence inside the WS-sphere. Using the  $1s$ -eigenfunction and  $f(\epsilon_{1s})$  we estimate that 0.365 electrons are transferred from the central ion to the neighboring ions in this case.

### 4. Fit formulae for the mean ionization $\bar{Z}$

In Fig. 2(a) the mean ionization of Be along four isotherms has been plotted. Fit formulae for  $\bar{Z}$  along six such isotherms are given below.

$$\bar{Z}(x) = \frac{(a_0 + a_1x + a_2x^2)}{(1.0 + b_1x + b_2x^2)}; \quad x = \bar{\rho} \text{ g/cm}^3 \quad (\text{A9})$$

The fit coefficients are given in Table I. The results for  $T = 150$ , and 155 eV provide a reasonable estimate of  $d\bar{Z}/dT$  near  $T = 150 - 155$  eV in parametrized form.

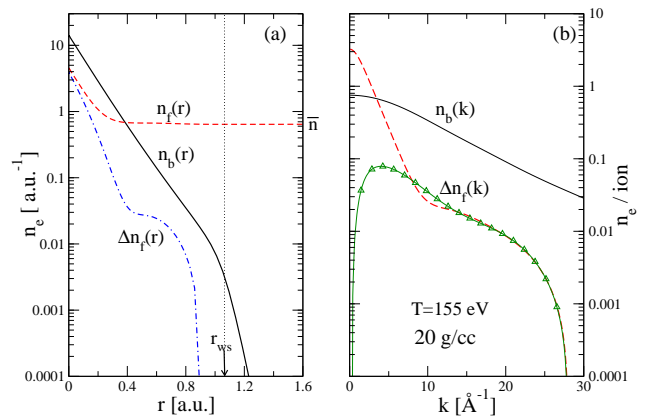


FIG. 6. (online color) (a) The bound and free electron densities from the NPA calculation. Here  $n(r) = n_b(r) + n_f(r)$  and  $\Delta n_f(r) = n_f(r) - \bar{n}$  are shown for Be at 20 g/cm<sup>3</sup> and  $T=155$  eV. Note that the bound-electron profile extends beyond  $r_{ws}$  and hence AA models that confine electrons to the Wigner-Seitz cell will differ from our calculations. (b) The Fourier transforms of these densities are displayed. They are used in calculating the “ion feature” and the Rayleigh weight of the XRTS profiles. The curve with triangles as data points shows the effect of a responding ion distribution (approximate two-component model) on the small- $k$  region.

TABLE I. Coefficients for  $\bar{Z}$  given by fit formula Eq. A9, for the density range 5 g/cm<sup>3</sup>-85 g/cm<sup>3</sup>. For  $T=1$  eV, and 10 eV,  $\bar{Z}$  jumps to 4.0 when  $\rho$  exceeds 80 g/cm<sup>3</sup>. Data on  $\bar{Z}$  calculated using the NPA for lower densities and other temperatures, as well as EOS data may be found in Ref. [24].

$T$ [eV]	$a_0$	$a_1 \times 10^2$	$a_2 \times 10^3$	$b_1 \times 10$	$b_2 \times 10^4$
155	3.77176	4.28122	-0.355843	0.232129	-2.03412
150	3.83327	6.30687	-0.501881	0.312884	-2.66131
100	3.61672	11.5306	-0.835117	0.571745	-4.80523
50	2.92788	26.3660	-1.13536	1.36315	-9.57148
10	1.98148	0.348542	0.100605	0.0	0.0
1	1.97952	0.343568	0.126261	0.0	0.0

### 5. The electron-ion pseudopotential and the ion-ion potential

A key component of these calculations is the construction of a weak  $s$ -wave electron-ion pseudopotential  $U_{ei}(k) = \Delta n_f(k)/\chi(k)$  that can be used in linear-response theory. Here  $\chi(k)$  is the full interacting e-e response function containing an LFC consistent with the finite- $T$  XC-potential used for e-e interactions. The pseudopotential is then used to construct the ion-ion pair-potential  $V_{ii}(k)$  and its Fourier transform  $V_{ii}(r)$  in real space. The latter can then be used in the HNC or MHNC equations, or in an MD simulation to obtain the ion-ion PDF. The pseudopotential  $U_{ei}(k)$  can be fitted approxi-

mately to a Heine-Abarankov form

$$U_{ei}(k) = -\frac{4\pi\bar{Z}}{k^2} \left[ D \frac{\sin(kr_c)}{kr_c} - (1-D) \cos(kr_c) \right]. \quad (\text{A10})$$

where  $k$  is in atomic units. We consider the case  $\bar{\rho} = 20$  g/cm<sup>3</sup>, and  $T = 155$  eV.,  $\bar{Z} = 3.247$  with  $k_F = 2.6704$  a.u. Then, for the range 0 to  $2k_F$ , the well-depth parameter  $D = 0.995835$ , while the core-radius  $r_c = 0.690797$ . As the electron response function  $\chi(k)$  drops rapidly for  $k > 2k_F$  the above parametrization is sufficient for most purposes. In our calculations we have, however, used the full numerical tabulation rather than the fitted forms.

Once the pseudopotential is obtained, the ion-ion pair-potential  $V_{ii}(k)$  can be obtained using linear-response theory. The  $r$ -space forms of the pair-potential can be fitted to a Yukawa-Friedel-tail form [58]. In the present case, a simple Yukawa form is found to be sufficient for  $r/r_{ws} \leq 4$ , with  $r_{ws} = 1.06427$  a.u.

$$V_y = (a_y/r) \exp(-k_y r). \quad (\text{A11})$$

The values of the fit parameters  $a_y, k_y$  for the case  $\bar{\rho} = 20$  g/cm<sup>3</sup>, and  $T = 155$  eV., are 12.8754 and 1.12975 respectively. The pair-potential at this high temperature state is not significantly oscillatory for  $r/r_{ws} > 4$ , behaving nearly as a Yukawa form with parameters  $a_y = 2.33447$ , and  $k_y = 0.710933$  for  $4 < r/r_{ws} < 8$ .

## 6. The calculation of $S_{ee}(k)$ within NPA and via a classical map

The NPA calculation yields continuum wavefunctions  $\psi_{kl}(r)$  with energies  $\epsilon_{kl} = k^2/2$ , and these can be used (instead of plane waves) to construct the electron response function  $\chi_{ee}(q, \omega)$  [45]. However, we explore below a simpler approach.

The NPA calculation replaces the many-electron e-e interaction by a one-body potential usually referred to as the XC-potential, together with the one-body Hartree potential. In effect, the interacting plasma is replaced by a *Lorentz plasma* where only the electron-ion interaction has to be dealt with, using the Kohn-Sham equation. The response function  $\chi(k)$  of the interacting electron fluid also simplifies in that the e-e local-field correction (LFC)  $G_{ee}(k)$  can also be expressed using a density derivative of the XC-potential. The Hartree potential reduces to zero for a uniform electron fluid (UEF), or for a two-component system (TCF) of electrons and ions forming a fluid of uniform density.

$$\chi_{ee}(k, \omega) = \chi_{ee}^0(k, \omega)/D_{ee}(k, \omega), \text{ UEF} \quad (\text{A12})$$

$$D_{ee}(k, \omega) = 1 - V_k \{1 - G_{ee}(k)\} \chi^0(k\omega) \quad (\text{A13})$$

As electrons obey quantum mechanics, obtaining the static structure factor  $S_{ee}(k)$  usually requires an evaluation of  $S_{ee}^0(k, \omega)$ ,  $G_{ee}(k, \omega)$  and an integration over  $\omega$ ,

even with the assumption that the LFC is independent of  $\omega$ . In the classical limit:

$$S_{ab}(k) = -\frac{T_{cf}}{\sqrt{n_a n_b}} \chi_{ab}(k, 0). \quad (\text{A14})$$

Hence  $\omega$  integrations etc., can be side-stepped by using a mapping [28] of the electrons to a classical Coulomb fluid, with the classical-fluid temperature  $T_{cf}$  defined by the following equations:

$$T_{cf} = \sqrt{(T^2 + T_q^2)} \quad (\text{A15})$$

$$T_q = E_F / (1.3251 - 0.1779\sqrt{r_s}) \quad (\text{A16})$$

The particles used in the classical map (cm) interact with a potential  $\phi_{ij}(r)$  consisting of a Coulomb interaction supplemented by a Pauli exclusion potential that exactly recovers the Fermi-hole in the e-e PDFs. The Coulomb interaction itself (represented by the operator  $1/r$ ) has a diffraction correction due to the quantum nature of the electrons. The non-interacting PDF, viz.,  $g_{ee}^0(r)$  and  $S_{ee}^0(k)$  are exactly known (Eqs. 3-5 of Ref. [28]).

The fully interacting  $S_{ee}(k)$  is obtained using  $\phi_{ij}(r)$  in an HNC equation or an MD simulation where  $T_{cf}$  is chosen so that the classical fluid has exactly the same XC-energy as the quantum electron fluid. Thus, since the Hartree energy is zero, the classical fluid and the quantum fluid have the same ground state energy and the same XC-energy. DFT states that, in that case the charge distributions should be the equilibrium charge distributions. It is shown in Ref. [28], and other publications [59, 60], that the  $g_{ee}(r), S_{ee}(k)$  and the total free energy obtained via this classical-map approach agree closely with results obtained by quantum Monte-Carlo and other microscopic methods. The CM-potentials, when used with an HNC equation to generate PDFs is referred to as the CHNC method. Alternatively MD may be used instead of the HNC equation. The HNC and MD procedures agree closely because the bridge-corrections needed in the 3D electron-fluid problem tend to be negligible even for very large values of the coupling parameter  $r_s$ , unlike in the case of the 2D-electron fluid [61].

The local-field correction  $G_{ee}(k)$  used in the NPA calculations is derived from the classical-map procedure via

$$G_{ee}(k) = 1 - (T_{cf}/\bar{n})(1/V_k) \{1/S_{ee}(k) - S_{ee}^0(k)\} \quad (\text{A17})$$

Hence the NPA calculation uses an interacting  $S_{ee}(k)$  which is exactly what is also given by the classical-map procedure. This  $S_{ee}(k)$  is displayed in Fig. 3(a) for  $\bar{\rho} = 7.5$  and 30 g/cm<sup>3</sup> at 155 eV. However, this  $S_{ee}(k)$  is the e-e structure factor for the spin-unpolarized uniform electron fluid in a non-responding medium. This is sufficient for addressing the XRTS signal for scattering wavevectors  $k_{sc} > k_F$  since the ion-density fluctuations which are ignored in the  $S_{ee}(k)$  of the UEF become relevant only at smaller  $k_{sc}$  values. Addressing smaller  $k_{sc}$  data requires a calculation of  $S_{ee}(k)$  that explicitly accounts for the two-component (electrons+ions) nature of the plasma [46].

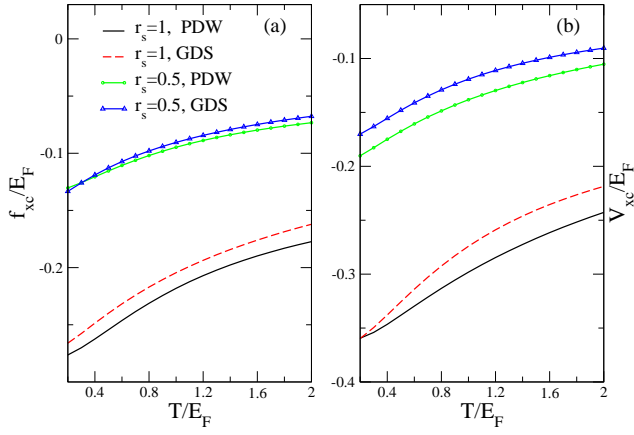


FIG. 7. (online color) (a) A comparison of the free-energy XC functionals of Perrot and Dharma-wardana [30], and that of Groth et al [43] in the range of densities ( $\rho$ ) indicated by the  $r_s$  parameter, and temperature  $t = T/E_F$ . The  $T = 0$  functional used in QMD calculations is also shown. (b) The XC-potentials  $V_{xc}(r_s, t)$  that enter into the Kohn-Sham calculations are displayed.

Extending the classical-map approach to electron-ion systems requires a theory for the effective temperature of the electron-ion interaction. Currently, this is a subject for further investigation.

### 7. Choice of finite- $T$ XC-functionals

QMD calculations that use  $N$ -atom DFT, with  $N \sim 64 - 512$  atoms, as implemented in large codes like the VASP [27] use the  $T = 0$  functional and do not implement a  $T$ -dependent e-e XC-functional. In the case of the NIF-Be,  $T = 155$  eV and densities are in the range  $20 \leq \bar{\rho} \leq 30$ . Hence we have  $0.719 \leq r_s \leq 0.635$  and  $1.59 \leq T/E_F \leq 1.25$  as the relevant range of  $r_s, t = T/E_F$  to be used in e-e XC-calculations. The XC-functional of PDW [30] for the Helmholtz free energy  $F(r_s, t)$  has been fitted to classical-map calculations within the range  $1 \leq r_s \leq 10$ , while the free energy fit of Groth et al (GDS) [43] used a wider range of data from PIMC and QMC calculations. A comparison of  $f_{xc}(r_s, t)$ , i.e., the XC-free energy per electron, and the corresponding  $V_{xc}(r_s, t)$  from the two parametrizations covering the region of interest in  $r_s, t$  are given in units of  $E_F$  in Fig. 7(a) and (b) respectively. It is seen that the two finite- $T$   $f_{xc}$ , and similarly the  $V_{xc}$  are in fair agreement. The Be calculations reported here (via the NPA code) implements the finite- $T$  PDW functional to capture e-e exchange and correlation effects.

The Kohn-Sham equations do not use the free-energy functional, but use the XC-potential defined by:

$$V_{xc}(r_s, t) = \frac{dF_{xc}(r_s, t)}{dn(r_s)} \quad (\text{A18})$$

Since  $F_{xc}(r_s, t)$  is given as a parametrized equation in

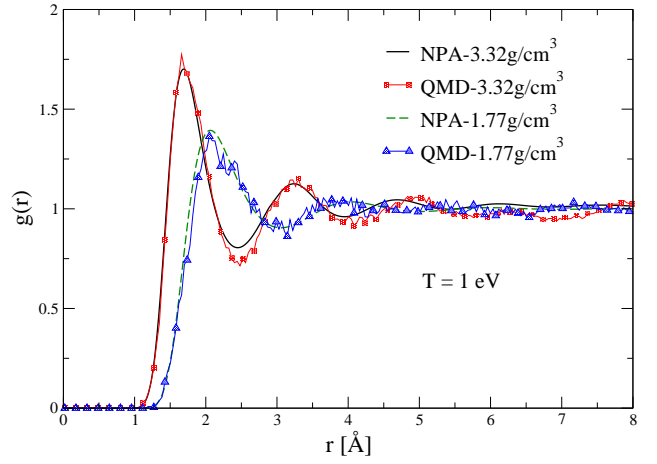


FIG. 8. (online color) The Be-Be  $g(r)$  for liquid-Be at  $\bar{\rho}=1.177$  and at  $3.282 \text{ g/cm}^3$  and  $T=1$  eV, calculated using the NPA and the MHNC-integral equation, compared with the PDF from QMD using the Vienna ab-initio simulation package (VASP).

$r_s, t$ , it is convenient to use an analytical derivative of the  $F_{xc}(r_s, t)$  fit. However, the analytic form of the derivative of the fit-form may not be adequate to reproduce the XC-potential in all regions of  $r_s, t$  although the fit reproduces the Helmholtz free energy. In fact, it is known that all the available fitted free-energy functionals, viz., PDW, Karasiev et al, and GDS fail to produce physically reasonable specific heats (where two temperature derivatives of the fit function are invoked) in certain ranges of  $r_s, t$  [62]. A method of directly evaluating the density derivative of the XC-potential obtained from the classical-map, without using a derivative of the fitted  $F_{xc}(r_s, t)$  is available from Eq. A17 for the local field correction to the electron-fluid response function. The same possibility exists for PIMC and QMC calculations. Hence an additional constraint can be placed on the analytic form of the  $V_{xc}(r_s, T)$  that has to be obtained from the fitted  $F_{xc}(r_s, t)$ . Additionally, the classical-map procedure can probably be contrived to directly evaluate  $V_{xc}(r_s, t)$ . Such developments are left for future work.

### 8. Comparison of PDFs obtained from NPA and VASP calculations

In Fig. 1 we compared NPA results with those of PIMC simulations to establish the extent of agreement that we have between the two methods. Here we further authenticate our NPA model for Be calculations by comparing the PDFs (Fig. 8) obtained for Be at  $1.117 \text{ g/cm}^3$ ,  $3.282 \text{ g/cm}^3$  at  $T=1$  eV with those from a QMD calculation using the VASP [26, 27]. Here the modified Hypernetted-chain (MHNC) equation has been used to calculate the PDFs using the ion-ion pair potential obtained from the NPA calculation.

Sixty four Be nuclei and 256 electrons were used in

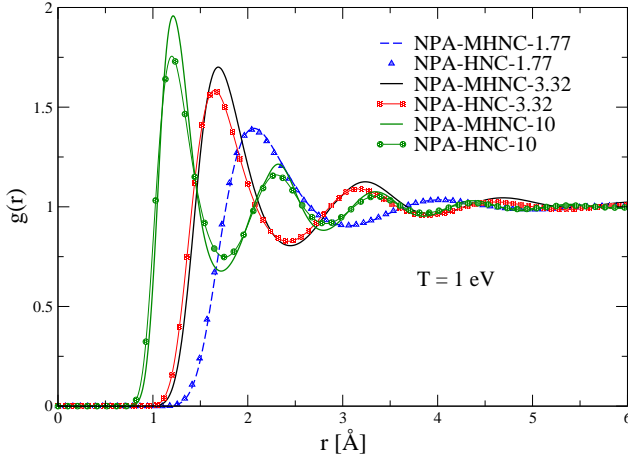


FIG. 9. (online color) The Be-Be  $g(r)$  for liquid-Be at  $\bar{\rho}=1.177$ , 3.282, and 10 g/cm<sup>3</sup> and  $T=1$  eV, calculated using the NPA ion-ion pair potentials, via the HNC and MHNC integral equation, where the latter includes bridge-diagram contributions modeled using Lado-Foils-Ashcroft theory [63].

an all-electron QMD simulation using VASP. An all-electron Be-pseudopotential supplied with the VASP was

used. An energy cutoff of  $\sim 260$  eV was employed. The (Monkhorst Pack)  $k$ -grid was used and calculations were done at the  $\Gamma$  point (0,0,0). Gaussian smearing (SMEAR=0) with a smearing of 0.1 eV was imposed, as recommended in Ref. [26]. The temperature was set using a Nosé-Hoover thermostat. The Perdew-Burke-Ernzerhof XC-functional [44] was used for electrons. It was ensured that the occupation in the highest energy state is less than 0.0001 even at the temperature (1 eV) studied for this comparison. This establishes the validity of our methods even in the low-temperature regime where strong-coupling effects are important.

In fig. 9 we compare the MHNC and HNC calculations for  $g(r)$  for three densities at 1 eV to establish the importance of bridge-graph contributions to ion-ion correlations at these densities at  $T=1$  eV. The bridge corrections are seen to be negligible for the low-density weakly-coupled case (1.117 g/cm<sup>3</sup>) studied here. Similarly, bridge corrections become unimportant for the temperatures relevant to the NIF experiment. The hard-sphere packing fraction  $\eta$  needed to satisfy the Lado-Foils-Ashcroft criterion [63] at 1 eV and 10 g/cm<sup>3</sup> is 0.43, while at 100 eV it becomes less than 0.03 and may be neglected.

- 
- [1] A. Ng, T. Ao, F. Perrot, M.W.C. Dharma-wardana, M.E. Foord, *Laser and particle beams*, **23**, 527-537 (2005).
  - [2] H Poole, M. K. Ginnane, M. Millot, H. M. Bellenbaum, G. W. Collins, S. X. Hu, D. Polsin, R. Saha, J. Topp-Muggleston, T. G. White, D. A. Chapman, J. R. Rygg, S. P. Regan, and G. Gregori. *Physical Review Research* **6**, 023144 (2024). DOI: 10.1103/PhysRevResearch.6.023144
  - [3] R.P. Drake, *High-Energy-Density Physics: Foundation of Inertial Fusion and Experimental Astrophysics*, Graduate Texts in Physics (Springer International Publishing, 2018).
  - [4] R. Betti, O. A. Hurricane, *Inertial-confinement fusion with lasers*, *Nature Physics* **12**, 435-448 (2016).
  - [5] J.A. Gaffney, Suxing Hu, P. Arnault..E. Zurek et al *High Energy Density Physics*, Aug 2018 <https://doi.org/10.1016/j.hedp.2018.08.00>
  - [6] E. E. McBride, A. Krygier, A. Ehnes, E. Galtier, M. Harmand, Z. Konôpková, H. J. Lee, H.-P. Liermann, B. Nagler, A. Pelka, M. Rödel, A. Schropp, R. F. Smith, C. Spindloe, D. Swift, F. Tavella, S. Toleikis, T. Tschentscher, J. S. Wark and A. Higginbotham. *Nature Phys.* **15**, 89-94 (2019).
  - [7] G. Gregori, S. H. Glenzer, W. Rozmus, R. W. Lee, and O. L. Landen. *Phys. Rev. E* **67**, 026412 (2003).
  - [8] S. H. Glenzer and Ronald Redmer, *Rev. Mod. Phys.* **81**, 1625 (2009).
  - [9] M.W.C. Dharma-wardana, Dennis D. Klug, and Richard C. Remsing *Phys. Rev. Lett.* **125**, 075702 (2020). doi: 10.1103/PhysRevLett.125.075702
  - [10] ! ref 10 M. W. C. Dharma-wardana, Dennis D. Klug, Hannah Poole and G.gregori. *arXive [cond-mat.mtrl-sci]*2408.04173 (2024).
  - [11] K. P. Driver, and B. Militzer, *Phys. Rev. Lett.* **108**, 115502 (2012).
  - [12] B. Militzer, K. P. Driver, *Phys. Rev. Lett.* **115**, 176403 (2015).
  - [13] L. Harbour, G. D. Förster, M. W. C. Dharma-wardana, and Laurent J. Lewis. *Phys. Rev. E* **97**, 043210 (2018).
  - [14] T. Döppner, M. Bethkenhagen, D. Kraus, P. Neumayer, D. A. Chapman, B. Bachmann, R. A. Baggott, M. P. Böhme, L. Divol, R. W. Falcone, L. B. Fletcher, O. L. Landen, M. J. MacDonald, A. M. Saunders, M. Schörner, P. A. Sterne, J. Vorberger, B. B. L. Witte, A. Yi, R. Redmer, S. H. Glenzer, and D. O. Gericke. *Nature* **618**, 270-275 (2023).
  - [15] A. N. Souza, D. J. Perkins, C. E. Starrett, D. Saumon, and S. B. Hansen. *PhysL Rev. E* **89**, 023108 (2014).
  - [16] K-U Plageman, H. R. Rüter, T. Bornath, Mohammed Shihab, Michael P. Desjarlais, C. Fortmann, S. Glenzer, R. Redmer. *Phys. Rev. E* **92**, 013103 (2015).
  - [17] L. Harbour, M. W. C. Dharma-wardana, D. Klug and L. Lewis. *Physical Review E* **94**, 053211, (2016).
  - [18] J. Vorberger, T. Preston, N. Medvedev, M. P. Bohme, Z. A. Moldabekov, D. Kraus, and T. Dornheim. *Phys. Lett.* **499**, 129362 (2024).
  - [19] M. W. C. Dharma-wardana, D. D. Klug, Hannah. Poole, and G. Gregori. *Phys. Rev. E* **111**(1) 015205 (2025). DOI:10.1103/PhysRevE.111.015205
  - [20] Mandy Bethkenhagen, Bastian B. L. Witte, Maximilian Schörner, Gerd Röpke, Tilo Döppner, Dominik Kraus, Siegfried H. Glenzer, Philip A. Sterne, and Ronald Redmer. *Phys. Rev. Research* **2**, 023260 (2020).
  - [21] T. Dornheim, T. Döppner, P. Tolias, M. P. Böhme, L.B. Fletcher, Th. Gawne, F. R. Graziani, D. Kraus, M. J. MacDonald, Zh. A. Moldabekov, S. Schwalbe, D.O. Gericke, and J. Vorberger. *arXive*:2402.19113v1



- [physics.plasmas-ph] (2024).
- [22] T. Dornheim, H. M. Bellenbaum, M. Bethkenhagen, S. B. Hansen, M. P. Böhme, T. Döppner, L. B. Fletcher, Th. Gawne, D. O. Gericke, S. Hamel, D. Kraus, M. J. MacDonald, Zh. A. Moldabekov, Th. R. Preston, R. Redmer, M. Schörner, S. Schwalbe, P. Tolias, and J. Vorberger. arXiv:2409.08591v1 [physics.plasmas-ph] (2024).
- [23] M. W. C. Dharma-wardana and F. Perrot. Phys. Rev. A **26**, 2096 (1982).
- [24] F. Perrot, Phys. Rev. E **47**, 570 (1993).
- [25] F. Perrot and M.W.C. Dharma-wardana, Phys. Rev. E. **52**, 5352 (1995).
- [26] Details for a standard MD simulation of *l*-Si using VASP are given in [https://www.vasp.at/wiki/index.php/Liquid\\_Si\\_-\\_Standard](https://www.vasp.at/wiki/index.php/Liquid_Si_-_Standard).
- [27] G. Kresse and J. Furthmüller, Phys. Rev. B **54**, 11169 (1996).
- [28] M. W. C. Dharma-wardana and F. Perrot, Phys. Rev. Lett. **84**, 959 (2000).
- [29] R. Bredow, Th. Bornath, W.-D. Kraeft, M.W.C. Dharma-wardana and R. Redmer Contributions to Plasma Physics, **55**, 222-229 (2015) DOI 10.1002/ctpp.201400080
- [30] F. Perrot and M. W. C. Dharma-wardana, Phys. Rev. B **62**, 16536 (2000); *Erratum*: **67**, 79901 (2003); arXiv:1602.04734.
- [31] Tobias Dornheim, Maximilian Böhme, Dominik Kraus, Tilo Döppner, Thomas R. Preston, Zhandos A. Moldabekov, and Jan Vorberger, Nature Communications **13**, 7911 (2022).
- [32] H. M. Bellenbaum, B. Bachmann, D. Kraus, Th. Gawne, M. P. Böhme, T. Döppner, L. B. Fletcher, M. J. MacDonald, Zh. A. Moldabekov, Th. R. Preston, J. Vorberger, and T. Dornheim. arXiv:2411.06830v1 [physics.plasmas-ph] (2024).
- [33] J. Chihara, J. Phys.: Condens. Matter **12**, 231 (2000).
- [34] M.W.C. Dharma-wardana and F. Perrot, Phys. Rev. A **45**, 5883 (1992).
- [35] T. Dornheim, T. Schoof, S. Groth, A. Filinov, and M. Bonitz. J. Chem. Phys. **143**, 204101 (2024)
- [36] W. Kohn, Phys. Rev. B **33**, 4331 (1986)
- [37] M.W.C. Dharma-wardana, Phys. Rev. E **104**, 015201 (2021).
- [38] G. Faussurier, C. Blancard, & M. Bethkenhagen. Phys. Rev. E **104**, 025209 (2021).
- [39] F. Perrot and M. W. C. Dharma-wardana, Phys. Rev. A **29**, 1378 (1984).
- [40] Thomas Gawne, Sam M. Vinko, and Justin S. Wark. Phys. Rev. E **103**, L023201 (2024).
- [41] V. Sharma and A. J. White, Phys. Rev. Lett. **134**, 095102 (2025).
- [42] Valentin V. Karasiev, James Dufty, S. B. Trickey, Phys. Rev. Lett. **120**, 076401 (2018).
- [43] S. Groth, T. Dornheim, T. Sjöström, F.D. Malone, W. Foulkes, M. Bonitz, Phys. Rev. Lett. **119** (13) 135001 (2017).
- [44] J. P. Perdew, K. Burke, and M. Ernzerhof, Phys. Rev. Lett. **77**, 3865 (1996).
- [45] M. W. C. Dharma-wardana, unpublished.
- [46] F. Perrot, Y. Furutani and M.W.C. Dharma-wardana, Phys. Rev. A **41**, 1096-1104 (1990).
- [47] M. W. C. Dharma-wardana, and François Perrot, Phys. Rev. E **58**, 3705 (1998).
- [48] L. Spitzer and R. Härm, Phys. Rev. **89**, 977 (1953).
- [49] M. W. C. Dharma-wardana (unpublished) preprint: <https://arxiv.org/abs/2404.19692>
- [50] P.A. Sterne, S.B. Hansen, B.G. Wilson, W.A. Isaacs, High Energy Density Phys. **3**, 278 (2007).
- [51] M. S. Murillo, J. Weisheit, S. B. Hansen, and M. W. C. Dharma-wardana, Phys. Rev. E **87**, 063113 (2013).
- [52] E. K. U. Gross, and R. M. Dreizler, *Density Functional Theory*, NATO ASI series, **337**, 625 Plenum Press, New York (1993).
- [53] J. Chihara, Phys. Rev. A **41**, 1247 (1991)
- [54] R. Piron and T. Blenski, Phys. Rev. E **83**, 026403 (2011).
- [55] S. X. Hu, L. A. Collins, V. N. Goncharov, J. D. Kress, R. L. McCrory, S. Skupsky. Physics of Plasmas, **23**, 042704 (2016).
- [56] Nadine Wette and J-C Pain, Phys. Rev. E **108**, 015205 (2023).
- [57] H. Umezawa, H. Matsumoto, and M. Tachiki. *Thermodynamic field dynamics and condensed states*, North-Holland, Amsterdam (1982).
- [58] M. W. C. Dharma-wardana, Lucas J. Stanek, and Michael S. Murillo Phys. Rev. E **106**, 065208 (2022).
- [59] J. Dufty, and Sandipan Datta. Phys. Rev. E **87**, 032101 (2013)
- [60] Yu Liu and Jianzhong Wu, J. Chem. Phys. **141** 064115 (2014).
- [61] François Perrot and M. W. C. Dharma-wardana, Phys. Rev. Lett. **87**, 206404 (2001).
- [62] V. Karasiev, S. B. Trickey and J. W. Dufty. Phys. Rev. B **99**, 195134 (2019).
- [63] F. Lado, S. M. Foiles and N. W. Ashcroft, Phys. Rev. A **26**, 2374 (1983).